



Numerical solution of duct flows of multiple visco-plastic fluids

M.A. Moyers-Gonzalez^{a*}, I.A. Frigaard^{a,b}

^a Department of Mathematics, University of British Columbia, 1984 Mathematics Road, Vancouver, BC, Canada V6T 1Z2

^b Department of Mechanical Engineering, University of British Columbia, 2324 Main Mall, Vancouver, BC, Canada V6T 1Z4

Received 31 July 2003; received in revised form 13 November 2003; accepted 15 December 2003

This article is part of a Special Volume containing papers from the XIIIth International Workshop on Numerical Methods in Viscoelastic Flows

Abstract

We consider numerical solution of duct flows of multiple visco-plastic fluids using both regularisation techniques and the augmented Lagrangian method. Using single fluid test problems, we demonstrate that there are certain classes of problems for which the augmented Lagrangian method is superior. These problems include those of determining the critical Bingham numbers and pressure gradients for which the flow stops, i.e. the yield limit. We then apply this method to two practical problems involving multiple fluids in ducts: multi-layer lubrication flows and counter-current exchange flows. Again we demonstrate the effectiveness of the augmented Lagrangian method for this type of problem.

© 2004 Elsevier B.V. All right reserved.

Keywords: Bingham fluid; Zero-flow limit; Multi-layer flow; Augmented lagrangian method

1. Introduction

In suitable dimensionless form, the axial flow of two visco-plastic (Bingham) fluids along a duct is modelled by the following system of equations:

$$\frac{\partial}{\partial x} \tau_{m,zx} + \frac{\partial}{\partial y} \tau_{m,zy} = -f, \quad (x, y) \in \Omega_m, \quad (1)$$

$$\frac{\partial}{\partial x} \tau_{c,zx} + \frac{\partial}{\partial y} \tau_{c,zy} = b - f, \quad (x, y) \in \Omega_c, \quad (2)$$

where the deviatoric stresses $\tau_{k,zj}$ are defined for $k = c, m$; $j = x, y$ by:

$$\tau_k > B_k \iff \boldsymbol{\tau}_k = (\tau_{k,zx}, \tau_{k,zy}) = \left[\mu_k + \frac{B_k}{|\nabla w|} \right] \nabla w \quad (3)$$

$$|\nabla w| = 0 \iff \tau_k \leq B_k, \quad (4)$$

with

$$\tau_k \equiv [\tau_{k,zx}^2 + \tau_{k,zy}^2]^{1/2}. \quad (5)$$

Here the duct has cross-section $(x, y) \in \Omega = \Omega_m \cup \Omega_c$, and the z -axis aligns with the direction of the flow, along the duct. The mathematical problem consists of finding the axial velocity $w(x, y)$. Dirichlet conditions are assigned at the boundary of Ω , the stress and velocity are continuous at the interface. It is assumed that each sub-domain has a Lipschitz continuous boundary. The parameters μ_k and B_k are the plastic viscosity and yield stress of fluid k , respectively; f denotes a modified axial pressure gradient and b is a buoyancy parameter.

Single phase flows of this type of materials were first considered by Bingham, [1], and later studied more extensively by Oldroyd [2], Prager [3], Mosolov and Miasnikov, [4,5], and by Duvaut and Lions [6]. Slightly more complex models are the Herschel–Bulkley and Casson models. These fluids occur both naturally and industrially; a range of different materials and description of many of the known analytical solutions of these equations is given in the review, [7].

The first motivation for studying the type of flow described by (1)–(4) is that there are a number of practical industrial examples of such multi-fluid flows. In particular, in oilfield cementing (both plug cementing and primary cementing) it is possible to find axial flows of two (largely) visco-plastic fluids. In this case the subscript m denotes a drilling mud and the

* Corresponding author. Tel.: +1 604 822 0297; fax: +1 604 822 6074.

E-mail address: mamgmex@math.ubc.ca (M.A. Moyers-Gonzalez).

superscript c denotes a cement slurry or spacer fluid. Flows of this type have been considered in [8–13]. Another class of interesting flows from an industrial perspective are multi-layer Poiseuille flows, such as occur in certain co-extrusion, lamination and coating processes. Whereas for most viscous–viscous fluid combinations, such fluids suffer from linear interfacial instabilities, it has been recently shown that use of yield stress fluids as lubricants can eliminate these, leading to both linear stability [14] and nonlinear stability [15].

The second motivation for considering the problem (1)–(4) is that it represents one of the simplest non-trivial examples of a multi-fluid visco-plastic flow. Such flows occur in displacement flows, in bubble propagation, in multi-layer flows, and a range of practical processing situations. These general flow scenarios bring in numerous computational challenges, which are not only specific to visco-plastic fluid flows, e.g. interface tracking, surface tension effects. The formulation (1)–(4) is sufficiently simple to avoid many of the complications of multi-dimensional multi-phase flows, but retains the key feature of a visco-plastic fluid, namely that of the yielding behaviour. Thus, in studying (1)–(4) we are able to observe whether the yield stress in itself presents any additional problem to the numerical solution of a multi-fluid problem.

The method that we use in this paper is the augmented Lagrangian method, as first introduced for this type of problem by Fortin and Glowinski, [16–18]. This method has been used occasionally in applications for computations of visco-plastic flows, e.g. [19,20], but in our opinion remains strangely under-utilised. The more popular alternative to the augmented Lagrangian method is to simply regularise the effective viscosity in (3) and (4), to remove the singularity at zero rate of strain. This approach was first advocated numerically in [17]. Probably the two most popular regularisations used are those of Bercovier & Engleman [21], and Papanastasiou [22]. These two regularised models have been implemented by a range of authors and for many different problems. A partial list of applications of viscosity regularisation is [9,13,23–30]. There are certainly advantages of the viscosity regularisation methods. A key one is their ease of application in commercially available computational fluid dynamics (CFD) software and other standard partial differential equation solvers.

The thesis that we wish to advance in this paper is not that the augmented Lagrangian approach is uniformly better than the regularisation approach, but rather that there exists a wide class of problems for which it is distinctly superior. The type of problem for which the augmented Lagrangian approach is advocated are those in which the yielding behaviour of the fluid(s) is critical. This class includes: (i) determining the critical yield limits of both single and multi-fluid flows; (ii) computing multi-fluid flows for which one (or more) of the fluids is unyielded, either at the interface or close to a wall. We shall encounter examples of these flows later. Also we shall show that in complex geometries the determination of critical yield limits is a difficult computational task, beset with pitfalls.

To close, we mention that regularisation and augmented Lagrangian methods are not the only methods that have been used for computational solution of visco-plastic flows. Different hybrid methods have also been developed, which often are very successful at capturing both yielded and unyielded fluid regions, but have limited scope for general application. Examples here are the *plug-forming* algorithm in [27], and the method in [31].

A brief outline of the paper is as follows. In Section 2 we address single fluid duct flows, for which the theory of determining the zero flow limits is well established. We show using the simplest example possible, a Poiseuille flow in a pipe, how the augmented Lagrangian method differs from the regularised methods in solving this type of flow problem. We then extend the computational method to more complex geometries and show how difficulties can arise. In Section 2 we consider multi-fluid problems in ducts. After a brief overview of how the augmented Lagrangian method extends to such problems, we tackle two test problems of practical importance. First we consider a lubrication flow, wherein we wish to establish how far from symmetry we can depart before the plug region is broken. Second, we consider a zero-flow limit for multiple fluids. Here the problem comes from oilfield plug cementing. The paper ends with a brief discussion.

2. Single fluid problems

For a single fluid, (i.e. $\Omega_s = \emptyset$), the background theory relating to existence and uniqueness of solutions and qualitative behaviour is developed in [4–6,17]. This class of flows includes some of the simplest known analytical solutions, e.g. Poiseuille flow in a circular pipe and in a plane channel. The variational formulation of these single fluid¹ Duct flow problems, consists of finding the unique minimiser $w \in H_0^1(\Omega)$ of the functional $J(u)$:

$$J(u) = \int_{\Omega} \frac{1}{2} |\nabla u|^2 + B |\nabla u| - fu \, dx, \quad u \in H_0^1(\Omega). \quad (6)$$

We are interested firstly in finding the solution of (6), which in general will be a computational task, (Section 2.2 below), and secondly in using this solution to determine the yield limit of a given flow, (Section 2.2).

2.1. Numerical solution methodology

It is known that there exists a unique solution to (6), as proven in [4,6]. However computationally, the main problem with the minimization (6) is the non-differentiability of $J(u)$ at $|\nabla u| = 0$, i.e. in unyielded regions. Thus, some form of relaxation or regularisation is needed. The main method

¹ For the single fluid problems in this section, we omit the subscript k denoting the fluid. We also rescale so that $\mu = \mu_m = 1$. Note that Dirichlet conditions are satisfied on the duct walls.

that we implement to circumvent this is the augmented Lagrangian method, (although we also implement a regularisation method for comparison). The augmented Lagrangian method is fully described in [16,18], wherein convergence and other results are also proven. Here we give only a brief outline, in order to describe its implementation and advantages. In place of (6) we consider the equivalent problem:²

$$\begin{aligned} & \min_{u \in H_0^1(\Omega), \mathbf{q} \in [L^2(\Omega)]^2: \mathbf{q} = \nabla u} J(u, \mathbf{q}) \\ & = \int_{\Omega} \frac{1}{2} |\mathbf{q}|^2 + B|\mathbf{q}| - fu \, dx. \end{aligned} \quad (7)$$

The idea now is to relax the constraint $\mathbf{q} = \nabla u$, by use of a Lagrange multiplier. Thus, we define the Lagrangian functional $L(u, \mathbf{q}, \lambda)$:

$$\begin{aligned} L(u, \mathbf{q}, \lambda) & = J(u, \mathbf{q}) + \int_{\Omega} \lambda \cdot (\mathbf{q} - \nabla u) \, dx, \\ u & \in H_0^1(\Omega), \mathbf{q}, \lambda \in [L^2(\Omega)]^2, \end{aligned} \quad (8)$$

and for $r > 0$ the augmented Lagrangian functional $L_r(u, \mathbf{q}, \lambda)$:

$$L_r(u, \mathbf{q}, \lambda) = L(u, \mathbf{q}, \lambda) + \frac{r}{2} \int_{\Omega} |\mathbf{q} - \nabla u|^2 \, dx. \quad (9)$$

The original minimisation problem (6) corresponds to finding a saddle point of $L(u, \mathbf{q}, \lambda)$. Since (6) admits a unique solution, there is a saddle point of $L(u, \mathbf{q}, \lambda)$ for which $\mathbf{q} = \nabla u$, and this will also be a saddle point of the augmented Lagrangian $L_r(u, \mathbf{q}, \lambda)$.

The algorithm that we adopt to find the saddle of $L_r(u, \mathbf{q}, \lambda)$ is described as ALG2 in [16]. In outline, given $u^n, \mathbf{q}^n, \lambda^n$:

- Fix \mathbf{q}^n, λ^n , and minimise with respect to u in the following functional,

$$\int_{\Omega} -fu + \frac{r}{2} |\nabla u|^2 - (r\mathbf{q}^n + \lambda^n) \cdot \nabla u \, dx \quad (10)$$

to find u^{n+1} .

- Fix u^{n+1}, λ^n , and minimise with respect to \mathbf{q} over Ω the following functional:

$$\int_{\Omega} \frac{1+r}{2} |\mathbf{q}|^2 + B|\mathbf{q}| - (r\nabla u^{n+1} - \lambda^n) \cdot \mathbf{q} \, dx \quad (11)$$

to find \mathbf{q}^{n+1} .

- Fix $\mathbf{q}^{n+1}, u^{n+1}$, and maximise with respect to λ to give λ^{n+1} , via the following update

$$\lambda^{n+1} = \lambda^n + \rho(\nabla u^{n+1} - \mathbf{q}^{n+1}). \quad (12)$$

² Loosely speaking, the space $L^2(\Omega)$ consists of functions that are square integrable over Ω ; $[L^2(\Omega)]^2$ is the space of vector functions, each of whose components are in $L^2(\Omega)$. The space $H_0^1(\Omega)$ consists of functions in $L^2(\Omega)$ that vanish on the boundary of Ω and whose first partial derivatives are also square integrable over Ω . More precise definitions can be found in any text on applied functional analysis.

Repeat above steps until convergence is achieved. Under the condition, (see [16]):

$$\rho < \frac{1 + \sqrt{5}}{2} r \quad (13)$$

we have the following convergence:

$$u^n \rightarrow w \quad \text{strongly in } H_0^1(\Omega), \quad (14)$$

$$\mathbf{q}^n \rightarrow \mathbf{q} \quad \text{strongly in } [L^2(\Omega)]^2, \quad (15)$$

$$\lambda^{n+1} - \lambda^n \rightarrow 0 \quad \text{strongly in } [L^2(\Omega)]^2, \quad (16)$$

$$\lambda^n \quad \text{is bounded in } [L^2(\Omega)]^2. \quad (17)$$

To explain informally the strong points of this method, note that in the first step of the algorithm, we are in fact solving the following linear Poisson equation:

$$0 = f + r(\nabla^2 u^{n+1} - \nabla \cdot \mathbf{q}^n) - \nabla \cdot \lambda^n, \quad x \in \Omega, \quad (18)$$

for the velocity u^{n+1} , with homogeneous Dirichlet boundary conditions. For this we use the finite element method, with piecewise linear elements on triangles for the velocity and piecewise constant approximations for \mathbf{q}^n and λ^n . For the minimisation with respect to \mathbf{q} , in the discrete setting we solve on each element

$$\min_{\mathbf{q}^{n+1}} \left\{ \left(\frac{1+r}{2} \right) |\mathbf{q}^{n+1}|^2 + B|\mathbf{q}^{n+1}| - \mathbf{M} \cdot \mathbf{q}^{n+1} \right\},$$

where $\mathbf{M} = \lambda^n + r\nabla u^{n+1}$. The solution is simply:

$$\text{If } |\mathbf{M}| \leq B \Rightarrow \mathbf{q}^{n+1} = 0 \quad (19)$$

$$\text{If } |\mathbf{M}| > B \Rightarrow \mathbf{q}^{n+1} = \theta \mathbf{M}, \quad (20)$$

where $\theta = (1 - B/|\mathbf{M}|)/(1 + r)$. Thus, our nonlinear non-differentiable minimisation is converted into an iterative sequence of linear Poisson equations and locally nonlinear equations, (in this case quadratic), both of which can be easily solved. Whilst the above are general advantages of this method, consider now the converged solution (purely formally), when $\mathbf{q} = \nabla u$. We see that (18) becomes:

$$\nabla \cdot \lambda = -f.$$

Thus, the converged λ is an admissible stress-field. Returning to the iteration for \mathbf{q} , we see that if $\mathbf{q} = \nabla u$, then where $\nabla u = 0$ the functional $\mathbf{M} = \lambda$. Thus, the criterion (19)–(20), distinguishing where $\mathbf{q} = 0$, converges to a yield criterion for the stress field λ .

For the regularisation method computations that we make comparisons with later, we simply replace the constitutive relation with

$$\tau_{ij}(\mathbf{u}) = \eta_{\epsilon}(\dot{\gamma}(\mathbf{u})) \dot{\gamma}_{ij}(\mathbf{u}) : \quad \epsilon \ll 1. \quad (21)$$

where $\eta_\epsilon(\dot{\gamma}(\mathbf{u}))$ is a regularised effective viscosity function, given here by

$$\eta_\epsilon = 1 + B \left(\frac{1}{[\epsilon^2 + \dot{\gamma}^2]^{1/2}} \right). \quad (22)$$

This particular choice is due to Bercovier and Engelman, [21]. We can see that the subyield stress behaviour is replaced in (22) by that of a very viscous Newtonian fluid as $\dot{\gamma} \rightarrow 0$. Using (21) and (22) the duct flow problem is simply a quasilinear Poisson equation to be solved on Ω . We again use piecewise linear triangular elements and a straightforward Picard-type iteration, computing the nonlinear part, (i.e. η_ϵ), using function values from the previous iteration.

2.2. Critical yield stresses and pressure gradients

Physically, it is obvious that for a fixed pressure gradient, if the yield stress is large enough then a single fluid will not flow in a duct, (or equivalently, a fixed yield stress requires a finite pressure gradient in order to initiate motion). For example, Hagen–Poiseuille flow in a pipe of radius 1 has the following simple analytical solution:

$$w(r) = \begin{cases} \frac{B}{2r^*}(1 - r^*)^2 & 0 \leq r \leq r^*, \\ \frac{B}{2r^*}[(1 - r^*)^2 - (r - r^*)^2] & r^* < r \leq 1, \end{cases} \quad (23)$$

r^* denotes the position of the yield surface. The expression (23) is valid only when $r^* \leq 1$. For $r^* > 1$ the solution is $w(r) = 0$. The yield surface position is related directly to the pressure gradient f and Bingham number B , by the following:

$$r^* = \frac{2B}{f}, \quad (24)$$

and hence we see that there exists a minimal pressure gradient, ($f > 2B$), or maximal Bingham number, ($B < f/2$), in order for the fluid to flow.

General consideration of this type of flow/no-flow threshold in a mathematical framework has been undertaken in [4,6]. Following [6], from the variational inequality associated with (6), it can be shown that the solution w satisfies

$$\int_{\Omega} |\nabla w|^2 \, d\mathbf{x} = \int_{\Omega} fw - B|\nabla w| \, d\mathbf{x}, \quad (25)$$

from which, if

$$K = \sup_{u \in H_0^1(\Omega); u \neq 0} \frac{\int_{\Omega} u \, d\mathbf{x}}{\int_{\Omega} |\nabla u| \, d\mathbf{x}}, \quad (26)$$

we see that we have no flow provided that:

$$f \leq \frac{B}{K}. \quad (27)$$

A more geometric approach is taken in [4]. Straightforwardly from (25), there is no flow (i.e. a non-trivial solution) in the

domain Ω if

$$\int_{\Omega} B|\nabla u| - fu \, d\mathbf{x} \geq 0 \quad (28)$$

for all $u \in H_0^1(\Omega)$. From [4], if u is a smooth function satisfying the boundary conditions, then

$$K' \int_{\Omega} |\nabla u| \, d\mathbf{x} \geq \int_{\Omega} u \, d\mathbf{x} : K' = \sup_{\Omega' \subseteq \Omega} \frac{\text{meas}(\Omega')}{\text{meas}(\partial\Omega')} \quad (29)$$

where Ω' is an arbitrary sub-domain of the domain Ω , with boundary $\partial\Omega'$, i.e. effectively the largest ratio of area to perimeter for a sub-domain of Ω . It is also shown in [4] that there exists a subdomain $\Omega' \subseteq \Omega$ that defines K' exactly. The boundary $\partial\Omega'$ of the optimal Ω' either coincides with that of Ω , or is the arc of a circle that is tangent with $\partial\Omega$ at common points. Thus, according to [4] the yield condition, for a non-zero flow in Ω , is that:

$$f \leq \frac{B}{K'}. \quad (30)$$

It would appear that $K = K'$, although a proof of this is lacking.

It is helpful to follow the methodology in [4] in order to get at least an intuitive feel for the relation between (26 and 29), and hence for what a Bingham fluid is “trying to do” in the zero flow limit. For this one should consider functions that approximately minimise (26). These functions are constant on as large a subdomain as is possible, but must drop to zero in a narrow ring close to the boundary. For such functions, the quotient in (26) can be approximately evaluated and is seen to relate to the geometric ratio in (29). The reader is referred to [4,6] for further details. In particular, [4] and the later paper [5] contain a wealth of interesting qualitative results concerning the shape and size of unyielded regions. For complex geometries, it is however impossible to obtain analytically the bounds on B (or f) for which the flow stops. Instead computation is needed. In this paper we examine the feasibility of adopting a naive approach of simply computing the axial flow at fixed Bingham, then increasing the Bingham number iteratively until the flow is observed to stop.

2.3. Stopping criteria for the Hagen–Poiseuille flow of a Bingham fluid

This is a classical and well known problem, the analytic solution of which has been given in (23) and the yield condition for flow to occur is, $f > 2B$. As illustration, we attempt to compute this yield boundary for the two different scenarios: (i) $f = 1$, B increasing; (ii) $B = 1$, f decreasing. Note that this is a one-sided limit, i.e. $w = 0$ for a finite range of parameters below the yield limit(s), so that it is natural to approach this limit from the flowing side, $w > 0$.

The first results that we present are the variation of $Q(w) = \int_{\Omega} w \, d\mathbf{x}$ with increasing B , (respectively f). These are presented for both the augmented Lagrangian computations and the regularised viscosity method, (here with $\epsilon = 10^{-5}$), see

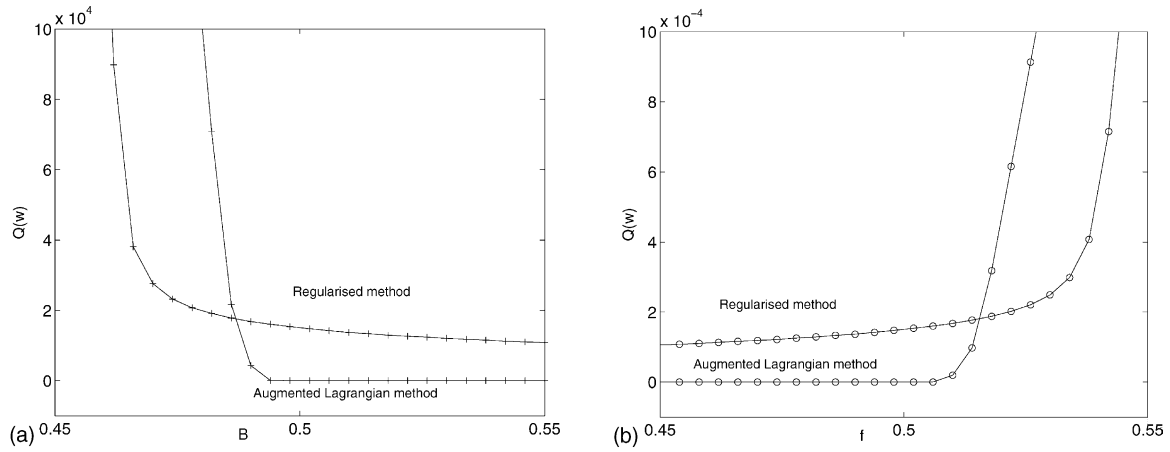


Fig. 1. Typical variation in $Q(w)$ as the yield limit is approached: (a) $f = 1$, increasing B ; (b) $B = 1$, increasing f ; regularisation parameter is $\epsilon = 10^{-5}$.

Fig. 1. These results illustrate immediately the drawback of the regularised method for this type of problem, i.e. for low shear the regularised method models a very viscous fluid, which therefore does not stop. Indeed, as we pass the zero flow limit, the regularised viscosity method computes a flow with viscosity B/ϵ and we expect that $Q(w) \propto \epsilon f/B$, which appears to approximately represent the behaviour in Fig. 1. We note that this trend is found (to lesser or greater degrees),

with other regularisations and values of ϵ . In contrast, the augmented Lagrangian method comes sharply to zero.

In order to illustrate clearly what the solutions look like, we present in Fig. 2 a sequence of computed velocity profiles for increasing B , with fixed $f = 1$. For Fig. 2a and b, we are still quite far from the yield limit. As B increases, the yield surface moves outward towards the wall. These results are computed using the augmented Lagrangian method, but at

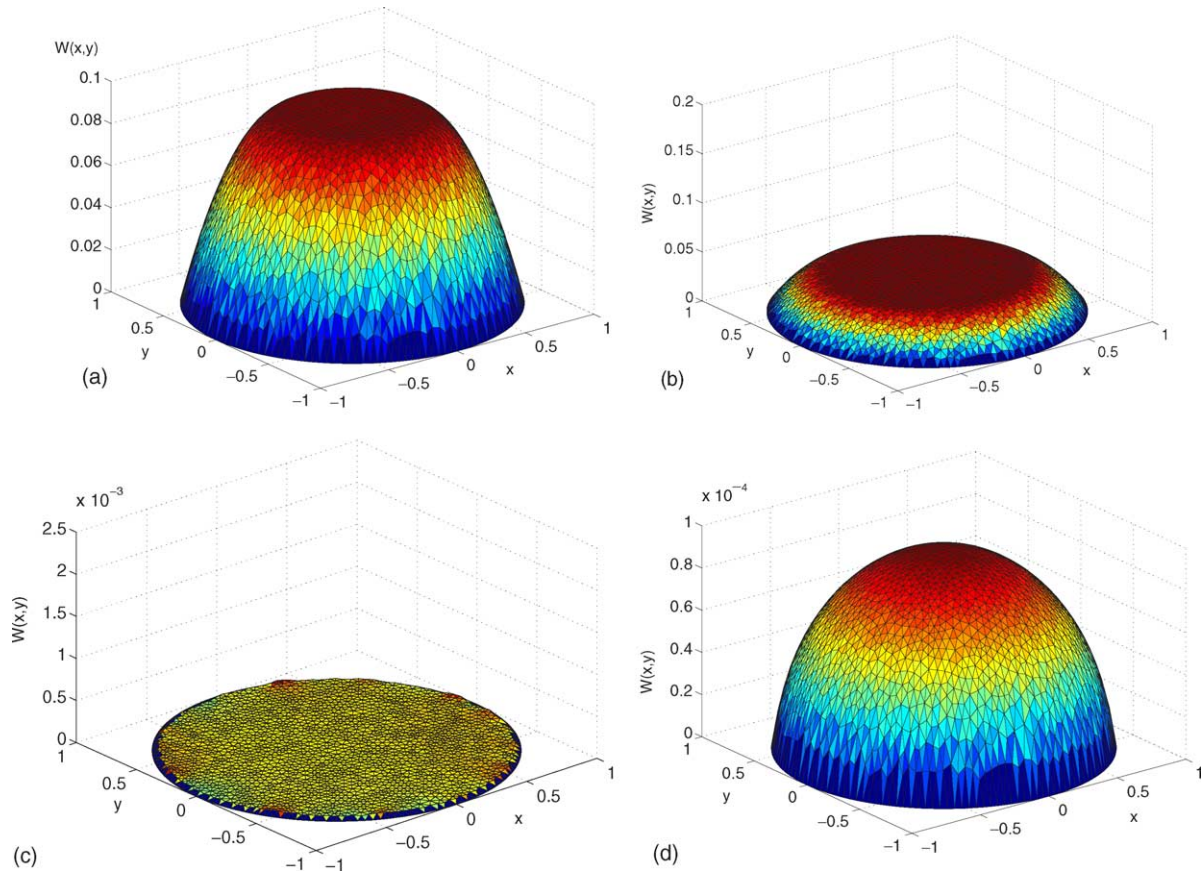


Fig. 2. Computed solution $W(x, y)$ for $f = 1$ and with varying B : (a) $B = 0.3$ (augmented Lagrangian method); (b) $B = 0.4$ (augmented Lagrangian method); (c) $B = 0.489$ (augmented Lagrangian method); (d) $B = 0.489$ (regularised method; $\epsilon = 10^{-5}$).

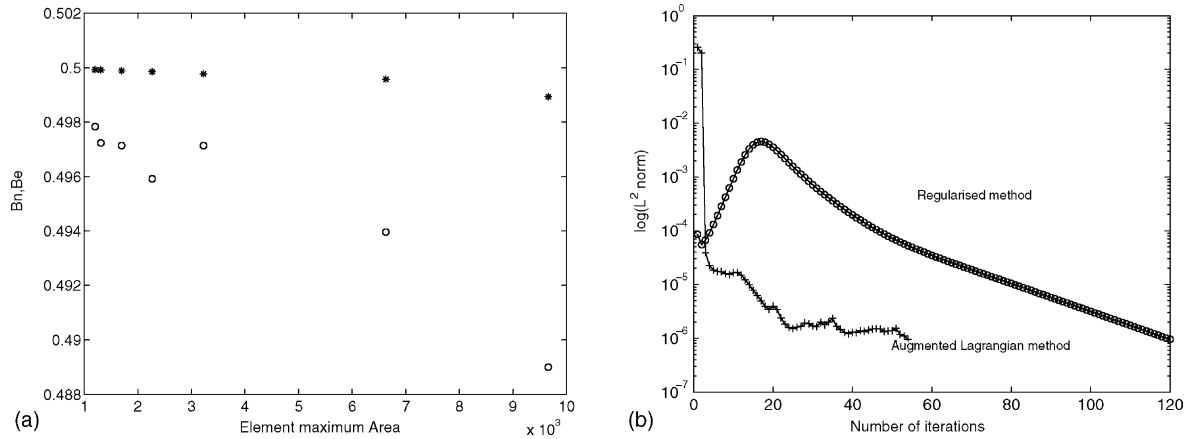


Fig. 3. (a) Computed zero flow limits B_n (○) for the flow in a pipe with different maximal mesh sizes; comparison with the theoretical bound of [4], (*); (b) comparison of convergence rates for the regularised method and augmented Lagrangian method.

these values of B , the regularised solution is also very close, both quantitatively and qualitatively. Fig. 2c and d show the velocity profiles just above the numerically computed zero flow limit, at the same Bingham number, for augmented Lagrangian and regularised methods respectively. The difference is very clear, whereas the augmented Lagrangian solution converges uniformly to zero, the regularised solution is purely viscous. Figs. 1 and 2 demonstrate clearly why the augmented Lagrangian method is the method of choice for such problems. It is unclear if the regularised method can be used at all for these problems.

It is also noticeable in Fig. 1a that the stopping value of B is in fact below the theoretical value $B = 0.5$, (and similarly in in Fig. 1b). This is due to the discretisation used. In the finite element method, the solution is obtained on a triangulation polygon which is an inner approximation to the circle. For this type of problem, this meshing error can be a significant factor, since the flow/no flow bounds are related directly to the geometry. In fact we can straightforwardly compute the area to perimeter ratio of our mesh, and hence compute a new exact limit for each mesh geometry. In Fig. 3a we show the comparison of computed numerical and exact zero-flow Bingham numbers, B_n and B_e , respectively, for a range of

different meshes. To find the zero-flow rate Bingham numbers we iterate with respect to B using the secant method with a tolerance of 10^{-5} , we find the zero-flow rate approximately when $Q(u) \sim 10^{-18}$. The horizontal axis plots the maximal element size h_{max} . The error appears to be $O(h_{max})$. In Fig. 3b we present for illustration the number of iterations of the two algorithms for convergence.

2.4. More complex geometries

Although it is possible to bound above and below the critical Bingham numbers (pressure gradients) for zero flow in arbitrary geometries, (see e.g. [4] for such bounds), exact evaluation requires computation. Here we present examples of two such computations for more complex geometries.

2.4.1. Square duct

The first problem considered is that of flow in a square duct, of side 1. The centre of the flow contains an unyielded plug region. As the Bingham number is increased from zero, we find that fluid becomes stuck in the corners of the duct. At still higher Bingham numbers the flow stops. For our computations, we fix $f = 1$ and increase B . In Fig. 4 we show the

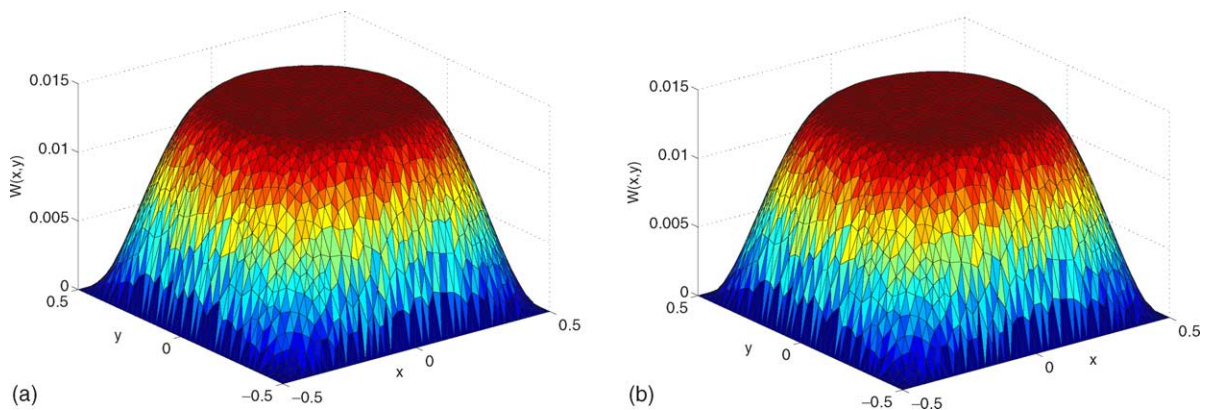


Fig. 4. Computed velocities $W(x, y)$ for the flow in a square duct at $B = 0.2$: (a) augmented Lagrangian method; (b) regularised method.

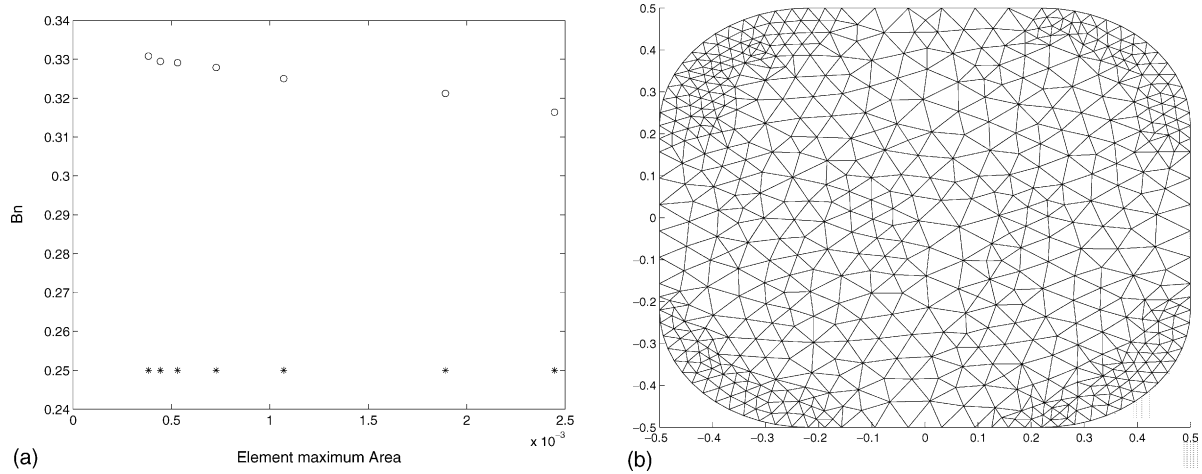


Fig. 5. (a) Computed zero flow limits B_n (\circ) for the flow in a square duct with different maximal mesh sizes; comparison with the theoretical bound of [4], (*). (b) The critical sub-domain $\Omega'_{d_{max}}$ on which the limiting solution of [4] is obtained.

flow at $B = 0.2$ for both the augmented Lagrangian and regularised methods. As with the pipe flow, as long as one is far from the zero flow limit, both methods produce reasonable (and consistent) approximations to the solution. For slightly larger B stagnant zones appear in the corners. The regularised method shows these as slowly moving whereas the augmented Lagrangian method computes the regions as static.

The critical pressure gradient for a square duct flow is considered in [4], who give the limit:

$$B = \frac{1}{2 + \sqrt{\pi}} \approx 0.2650 \dots$$

This value is easily found by considering the maximum over d of the ratio of area to perimeter for subdomain Ω'_d that consist of the square with corners replaced by quarter circles of radius d , i.e. a rounded-off square, say $\Omega'_{d_{max}}$. In Fig. 5a we show for a range of different mesh sizes our attempts to attain the critical limit numerically, $B = B_n$. The limit appears to converge to $B_n \approx 0.33 \dots$, which is far above that of [4].

Apart from being in error, it may seem strange that different zero flow limits are found for different discretisations when the flow domain is regular. Note however, that the triangular discretisation of the square does not well approximate the shape of the critical sub-domain $\Omega'_{d_{max}}$ for which the flow stops. It is this discretisation error that accounts for the variation in computed B_n , (as well as solution errors of course). Fig. 5b shows the critical subdomain $\Omega'_{d_{max}}$. At the points of tangency of the circular arcs with the sides of the square, it is impossible to discretise the regions external to $\Omega'_{d_{max}}$ with a triangulation, without violating the cone conditions.

Since the limiting flows consist of static regions external to $\Omega'_{d_{max}}$, it would appear that the limiting solutions satisfy the Dirichlet problem on $\Omega'_{d_{max}}$. In other words, the critical Bingham numbers for $\Omega'_{d_{max}}$ and Ω are identical. As illustrated in Fig. 5b, there is no difficulty in discretising $\Omega'_{d_{max}}$. We can therefore solve the duct flow problem on $\Omega'_{d_{max}}$ and determine the zero flow limit on $\Omega'_{d_{max}}$. In Fig. 6a we show an example

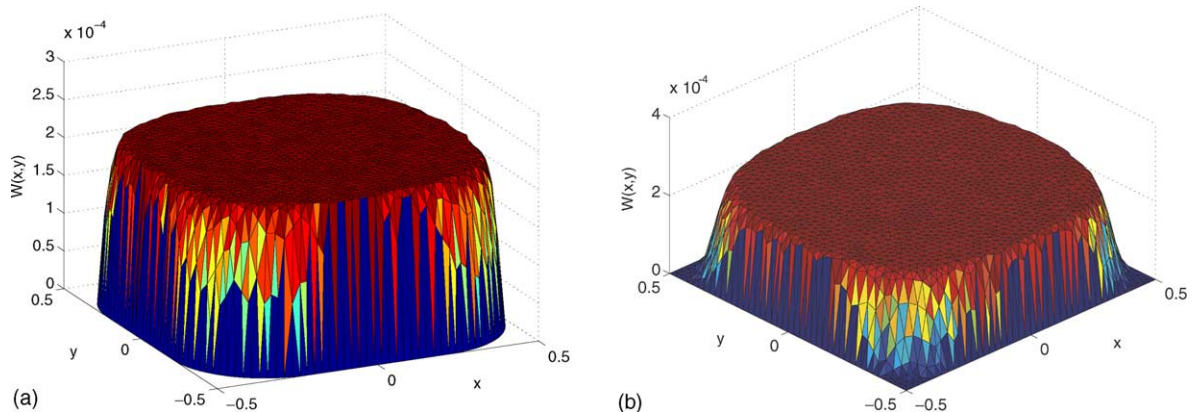


Fig. 6. (a) Computed solution $W(x, y)$ on $\Omega'_{d_{max}}$ at $B = 0.25$. (b) Computed solution on Ω at $B = 0.25$

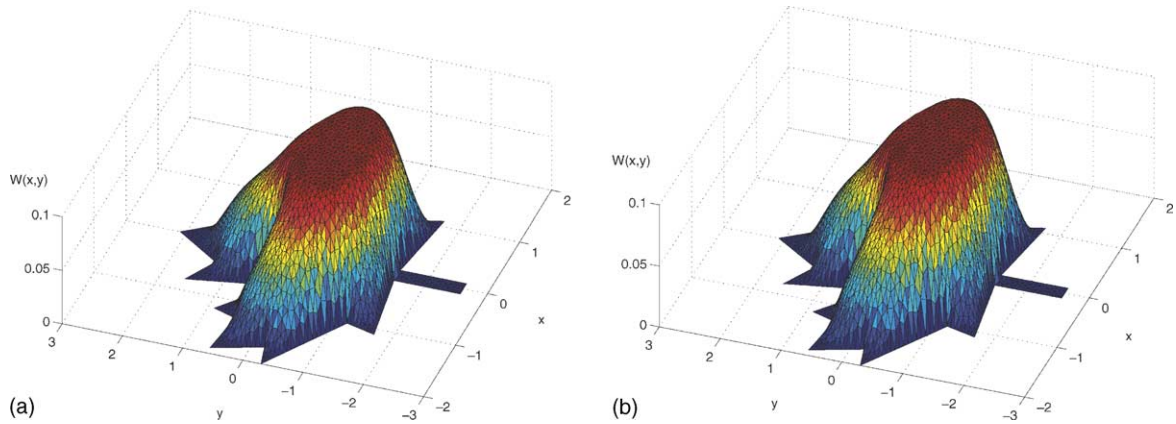


Fig. 7. Computed velocities $W(x, y)$ for the flow in a maple leaf shaped duct at $B = 0.3$: (a) augmented Lagrangian method; (b) regularised method.

of a velocity profile computed on $\Omega'_{d_{max}}$ at $B = 0.25$, and in Fig. 6b we plot the solution computed on the full square. Soon above this value, the solution drops to zero. The difficulty of discretisation on the square domain, to approximate $\Omega'_{d_{max}}$ from outside, is self-evident.

Thus, the results of this section illustrate that even for relatively simple domains determination of the critical Bingham numbers is a non-trivial problem. Use of the augmented Lagrangian method does at least mean that flows do actually stop, but there are still significant problems in approximation. The latter are related to the discretisation itself, rather than the choice of algorithm with which to solve the equations. In practice of course, for a general region Ω one does not know the critical sub-domain. Thus, although here we have been able to verify the results of [4], in general for a complex domain we are unlikely to be able to successfully determine the zero flow limits in the way we have, i.e. some a priori knowledge or intuition regarding the yield surfaces is still required.

2.4.2. Maple leaf

To emphasise the above points, we include one further complex example. The duct that we have chosen has a cross-section in the form of a maple leaf. Although there is some symmetry in the duct, there are a number of corner regions in which the fluids are likely not to flow. Determination of the zero flow limit analytically would be difficult. In Fig. 7 we show for comparison, two velocity solutions computed using the augmented Lagrangian and the regularisation method, at a Bingham number far below that for which the flow stops. We can see that the velocities are similar and that in certain constricted regions of the maple leaf there is essentially no flow.

As we increase the Bingham number, using the augmented Lagrangian method, the velocity decays to zero. However, the limit is very difficult to determine and is very sensitive to the mesh. In Fig. 8 we show an example of one of the meshes and of the different numerical yield limits computed for different meshes. For the duct shape in Fig. 8a the re-entrant

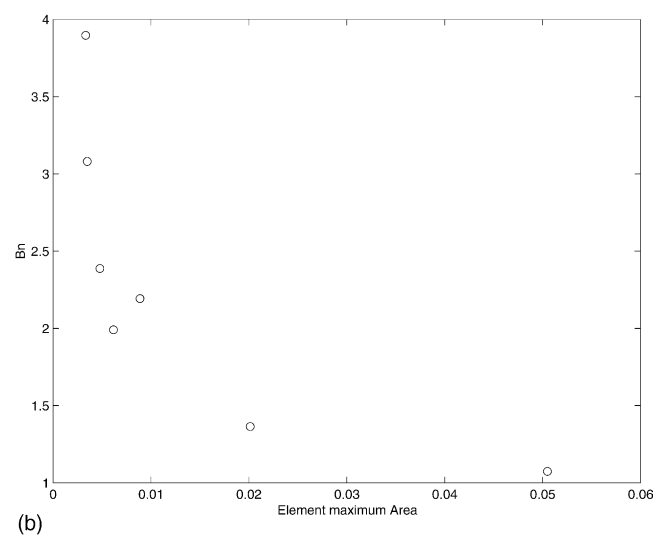
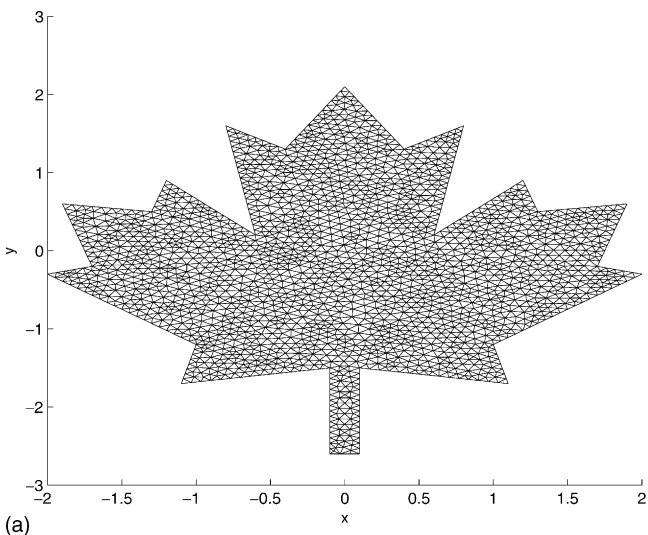


Fig. 8. (a) An example mesh for the maple leaf geometry. (b) Variations in the computed yield limit with maximal mesh size.

corners are problematic for approximation. It is likely that the optimal shape will consist of a sequence of arcs, tangent to the perimeter in each leaf of the maple leaf. Each of these will be impossible to approximate using triangular elements satisfying a cone condition. This partly accounts for the large variability in computed yield limit. Certainly, computational results with the variability of those in Fig. 8b can not be relied upon. It is unclear how problems such as this should be tackled computationally.

Before progressing to multi-fluid problems, we note that for problems of the type considered here and in Section 2.4.1, adaptive meshing techniques are certainly advisable. Here we refer in particular to the recent work of Roquet and Saramito, [32].

3. Multi-fluid problems

For multiple fluids duct flows, the variational formulation can be obtained in analogous fashion to that for a single fluid. The momentum equations are multiplied by a test function and integrated over each fluid domain separately. Use of the divergence theorem and summing over the two fluid domains to cancel out boundary integrals leads to the following variational inequality:

$$\begin{aligned} & \mu_k \sum_{k=c,m} \int_{\Omega_k} \nabla w \cdot \nabla(v-w) + B_k |\nabla v| - |\nabla w| \, dx \\ & \geq f Q_m(v-w) + (f-b) Q_c(v-w), \end{aligned}$$

$$\forall v \in H_0^1(\Omega), \quad w \in H_0^1(\Omega)$$

see e.g. [9]. This problem is equivalent to finding the unique minimiser $w \in H_0^1(\Omega)$ of the functional $J(u)$:

$$\begin{aligned} J(u) = & \sum_{k=c,m} \int_{\Omega_k} \frac{\mu_k}{2} |\nabla u|^2 + B_k |\nabla u| \, dx - f Q_m(u) \\ & - (f-b) Q_c(u), \quad u \in H_0^1(\Omega), \end{aligned} \quad (31)$$

where

$$Q_k(u) = \int_{\Omega_k} u \, dx, \quad u \in H_0^1(\Omega), \quad k = c, m.$$

Results related to existence and uniqueness of solutions are derived in [9]. The functional $J(u)$ has similar properties to that of the single fluid problem. Thus, many of the methods applicable to the single fluid problem may be generalised. In particular, the augmented Lagrangian method can be readily applied, as we outline below. Thereafter, we consider two multi-fluid problems of practical importance. In Section 3.2 we consider visco-plastically lubricated flows, and in Section 3.3 we consider exchange flows. An overview of the background to each problem is given in each section.

3.1. Augmented Lagrangian algorithm for multi-fluid problems

As in Section 2.1 we relax $J(u)$ by setting $\mathbf{q} = \nabla u$, and incorporate this constraint via a Lagrange multiplier term and a quadratic penalty term. In brief, we solve the saddle point problem:

$$\max_{\lambda} \min_{u, \mathbf{q}} L_{\mathbf{r}}(u, \mathbf{q}, \lambda) : u \in H_0^1(\Omega), \mathbf{q}, \lambda \in [L^2(\Omega)]^2, \quad (32)$$

where

$$\begin{aligned} L_{\mathbf{r}}(u, \mathbf{q}, \lambda) = & \sum_{k=c,m} \int_{\Omega_k} \frac{\mu_k}{2} |\mathbf{q}|^2 + B_k |\mathbf{q}| \, dx \\ & - f Q_m(u) - (f-b) Q_c(u) \\ & + \sum_{k=s,m} \int_{\Omega_k} \frac{r_k}{2} |\mathbf{q} - \nabla u|^2 + \lambda \cdot (\mathbf{q} - \nabla u) \, dx. \end{aligned} \quad (33)$$

We solve this using the same iterative Uzawa algorithm as in Section 2.1, (i.e. with the above modifications). ALG2 for our problem is:

- Fix \mathbf{q}^n, λ^n minimise with respect to u in the following functional,

$$\begin{aligned} & \int_{\Omega_m} -fu + \frac{r_m}{2} |\nabla u|^2 - (r_m \mathbf{q} + \lambda) \cdot \nabla u \, dx \\ & + \int_{\Omega_c} -(f-b)u + \frac{r_c}{2} |\nabla u|^2 - (r_c \mathbf{q} + \lambda) \cdot \nabla u \, dx \end{aligned} \quad (34)$$

to find u^{n+1} .

- Fix u^{n+1}, λ^n minimise with respect to \mathbf{q} over $\Omega_m \cup \Omega_c$ the following functional:

$$\begin{aligned} & \int_{\Omega_m} \frac{1+r_m}{2} |\mathbf{q}|^2 + B_m |\mathbf{q}| - (r_m \nabla u^{n+1} - \lambda^n) \cdot \mathbf{q} \, dx \\ & + \int_{\Omega_c} \frac{1+r_s}{2} |\mathbf{q}|^2 + B_c |\mathbf{q}| - (r_c \nabla u^{n+1} - \lambda^n) \cdot \mathbf{q} \, dx \end{aligned} \quad (35)$$

to find \mathbf{q}^{n+1} .

- Fix $\mathbf{q}^{n+1}, u^{n+1}$ maximise with λ to give λ^{n+1} , via the iterative update:

$$\lambda^{n+1} = \lambda^n + \rho_k (\nabla u^{n+1} - \mathbf{q}^{n+1}), \quad (36)$$

We observe that the above algorithm is essentially the same as for the single fluid problem in Section 2.1. The classical form of the velocity problem is to find u from:

$$0 = f + r_m (\nabla^2 u - \nabla \cdot \mathbf{q}) - \nabla \cdot \lambda \quad x \in \Omega_m$$

$$0 = (f-b) + r_c (\nabla^2 u - \nabla \cdot \mathbf{q}) - \nabla \cdot \lambda \quad x \in \Omega_c$$

with continuity of u at the interface Γ and also

$$[r_k(\nabla u - \mathbf{q}) \cdot \mathbf{n} - \lambda \cdot \mathbf{n}]_{\Gamma^-}^{\Gamma^+} = 0, \quad (37)$$

(Γ^+ and Γ^- denoting the two sides of the interface). From the above we see again the interpretation of the converged λ as an admissible stress field, now with normal component continuous across the interface, as would be expected physically.

Different penalty weights r_k , $k = c, m$ are included above, and in updating λ different over-relaxation parameters ρ_k , $k = c, m$, can be used. It is worth noting that the convergence conditions are analogous to those for the single fluid case, which may seem surprising. However, this is simply because they are based upon the minimisation of (31), which is one of a general class of functionals for which the method can be applied. These results also relate to conditions for convergence, rather than speed of convergence. As with the single fluid case, this is found to be sensitive to choice of r_k , $k = c, m$ and ρ_k , $k = c, m$. It is not clear how to do this optimally. After several tries, a robust choice for r_k and ρ_k appears to be $r_c = r_m = 1$ and $\rho_k = r_k$.

Insofar as numerical details go, we discretise on triangular finite elements, using piecewise linear basis functions for u and piecewise constant basis functions for λ and \mathbf{q} . The mesh is aligned with the fluid-fluid interface, ensuring continuity of u directly. The condition (37) becomes a natural condition at the interface, (i.e. it is handled automatically within the finite element method). Solution of the u problem at each iterate involves solving a Poisson equation. The matrix inversion is handled using a Gauss-Seidel iteration. For the minimisation with respect to \mathbf{q} , we proceed as in Section 2.1, by solving an algebraic equation on each element, (essentially (19) and (20) with subscripts). The λ update needs no explanation.

3.2. Visco-plastic lubrication flows

When two fluids of differing viscosity flow together in a parallel flow along a duct, the interface between the fluids can be linearly unstable at low Reynolds numbers, see e.g. [33–44]. Such instabilities are obviously detrimental to the use of this type of flow for any type of manufacturing process. In the case where one of the fluids is visco-plastic, the flow can be much more stable. The type of configuration that we consider is that shown schematically in Fig. 9. The outer fluid is a visco-plastic and the inner fluid is viscous, (or possibly visco-plastic). The critical features are that the outer fluid maintains a yield surface at the interface and that the fluid is represented as having a true yield surface, (i.e. no regularisation).

In [14] it is shown that this type of flow configuration is linearly stable, even at large Reynolds numbers. Maintenance of an unyielded region at the interface is critical to this. For example, regularised models, such as those studied in the two-layer flow of [44], exhibit low Reynolds number linear instabilities. Equally, the reverse configuration, (Newtonian fluid outside of Bingham fluid), which has been studied in

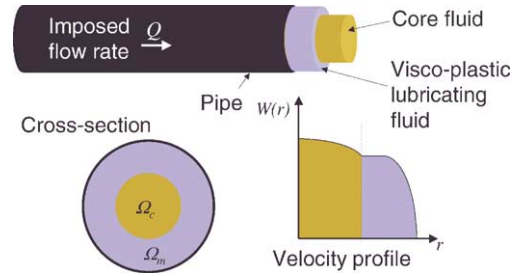


Fig. 9. Schematic of the visco-plastic lubrication configuration.

one dimension in [45], will also be unstable at the interface in multi-dimensions. Very recently, the linear stability results in [14] have been extended in [15] to nonlinear stability, including motion of the central core region in Fig. 9. Critical to these later results is the argument that a small perturbation of the basic flow from its axisymmetric position will still preserve an unyielded plug region around the central region. Although this can be established from continuity arguments, the degree of asymmetry at which the outer plug breaks is easier to compute directly. Also if one wishes to establish sharp estimates for stability, it is necessary to evaluate these plug-breaking limits more exactly than can be done analytically

In Fig. 10a–c, we show a sequence of velocity profiles computed using the augmented Lagrangian method. The inner fluid region has radius $r_i = 0.3$, and we take both fluids to be Bingham fluids with Bingham numbers $B_c = 0.5$ and $B_m = 4$ (outer fluid). The modified pressure gradient is $f = 11.9445$ and the buoyancy parameter is $b = 5.97225$. After rescaling we can set $\mu_s = 1$ and $\mu_m = m$, where m is the plastic viscosity ratio, which we set equal to 1. The fully concentric solution can be computed analytically, but as symmetry is broken numerical solution is necessary. We show velocity profiles with the centre of region Ω_c displaced to $(x_s, 0)$ where $x_s = 0.1, 0.3, 0.4$. It can be seen that for small x_s the unyielded plug region remains intact, but eventually yields.

In Fig. 10d we show how the minimal width of the unyielded plug region separating the two fluids decays with increasing eccentricity x_s . It is this type of computation that is needed if sharper stability bounds than those in [15] are to be established. We note that computation of this type of yield limit, which is based on a non-zero flow, is likely to be fairly stable with respect to variations in mesh.

3.3. Exchange flows

The second example problem we consider arises in the industrial process of plug cementing of oil wells. The model involves (1)–(4) with buoyancy $b = 1$. The flow is in a circular domain of unit diameter and with the additional constraint

$$\int_{\Omega} w \, d\Omega = 0, \quad (38)$$

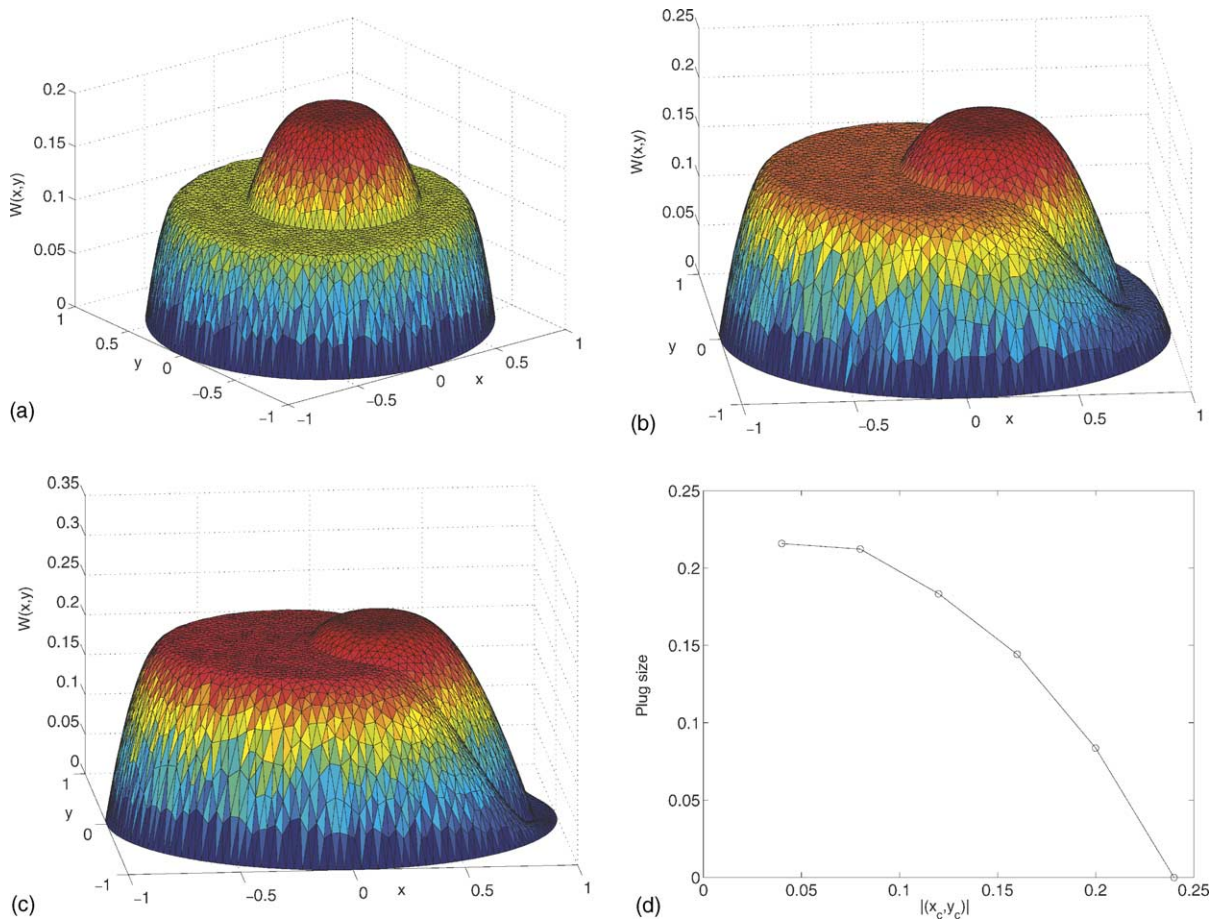


Fig. 10. Velocity profiles for visco-plastic lubrication flows; parameters $r_i = 0.3$, $B_c = 0.5$, $B_m = 4$, $f = 11.9445$, $b = 5.97225$: (a) $x_s = 0.1$, (b) $x_s = 0.3$, (c) $x_s = 0.4$, (d) decay of minimal width of unyielded plug with x_s .

i.e. there is no net flow along the duct. In this process one places a heavy fluid, a cement slurry, on top of a lighter fluid, either a drilling mud or a viscous pill, in an inclined closed-ended pipe, the oil well, see Fig. 11. The aim of the process is that the cement slurry remains static for a period of hours, while it hardens and forms a solid *plug* in the well, which either hydraulically seals the well, (an *abandonment plug*), or is used during drilling to redirect the path of the well, (a *kick-off plug*).

The key question here is how large must the yield stresses be in order for the plug to remain static. In yard tests using representative oilfield fluids and pipe sizes, and with cement placed above mud in an inclined pipe, (see e.g. [46]), in those cases where the rheologies of the fluids were somehow *close* to being statically stable, the cement slurry is observed to slump towards the lower side of the pipe and move slowly downwards in an axial direction, displacing the lighter drilling mud upwards, (as shown in Fig. 11). This is observed to be a slow, stable laminar flow. Qualitatively similar results have also been observed in a series of experiments performed using visco-plastic laboratory fluids, reported in [11]. During this motion, the interface between the two fluids remains well defined and elongates during the slumping motion. Apart

from close to the ends of the propagating displacement fronts, the interface and velocity field of both fluids is essentially parallel to the pipe axis.

The above situation forms the basis for the model (1)–(4) and (38), which is derived in some detail in [8,9], i.e. we have

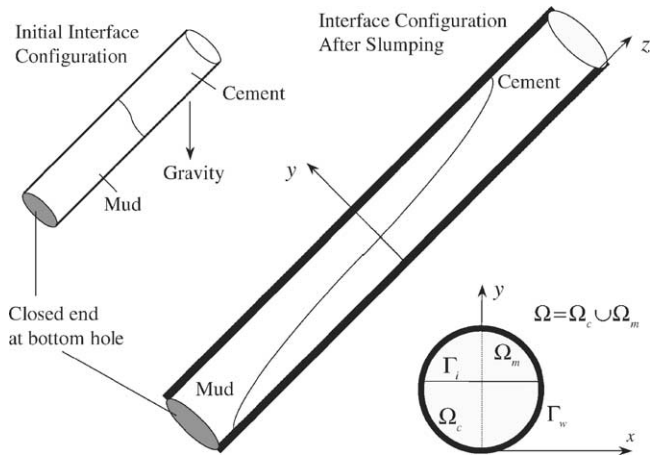


Fig. 11. Schematic of the plug cementing process.

a buoyancy driven axial flow, driving the cement downwards and the mud upwards. The question of how large the yield stresses must be in order to stop this axial flow is addressed in [13], and we summarise the chief results from [13] below. The methods used in [13] are mostly analytical, considering what happens close to the static solution. Indeed a deficiency of the results in [13] is that it has not been possible to verify them computationally for non-trivial interface configurations. A regularisation method was used in [13] to explore certain features of these flows, but for the all important determination of critical yield stresses limits, it proves inadequate.

The typically observed interface configuration in a cross-section of the pipe is a horizontal interface at some height h above the bottom of the pipe, i.e. the fluids are stratified with the lighter mud flowing upwards as the heavier cement flows downwards. The geometry is described by the various cross-sectional areas and perimeter fractions, expressed as a function of h .

$$\alpha_c(h) = 1 - \alpha_m(h) \equiv \frac{1}{\pi}(\cos^{-1}(1 - 2h) - 2(1 - 2h)[h(1 - h)]^{0.5}), \quad (39)$$

$$s_c(h) = 4 - s_m(h) \equiv \frac{4}{\pi} \cos^{-1}(1 - 2h), \quad (40)$$

$$s_i(h) \equiv \frac{8}{\pi}[h(1 - h)]^{0.5}. \quad (41)$$

These are illustrated in Fig. 12. Geometrically, the functions α_c and α_m are the area fractions of Ω_c and Ω_m , respectively; s_c , s_m and s_i are the lengths of the boundaries $\Gamma_{c,w}$, $\Gamma_{m,w}$ and Γ_i , each divided through by $\pi/4$. These functions are plotted in Fig. 13.

The curve in the $(\tau_{c,Y}, \tau_{m,Y})$ -plane above which the only solution of (1)–(4) and (38) is $w = 0$, is defined by:

$$\sup_{h \in [0,1]} F(h, \tau_{c,Y}, \tau_{m,Y}) = 0, \quad (42)$$

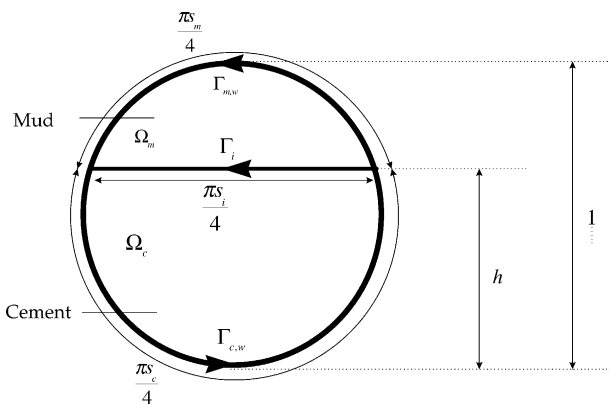


Fig. 12. Schematic of the geometry for an exchange flow with the fluids separated by a horizontal interface.

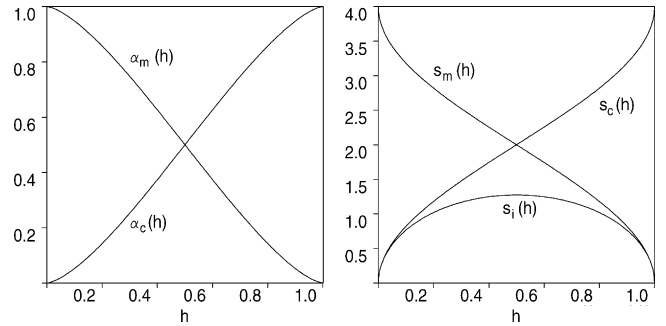


Fig. 13. The functions $\alpha_c(h)$, $\alpha_m(h)$, $s_c(h)$, $s_m(h)$ and $s_i(h)$.

where

$$F(h, \tau_{c,Y}, \tau_{m,Y}) = \beta_0(h) - \beta_m(h)\tau_{m,Y} - \beta_c(h)\tau_{c,Y} - \min\{\tau_{k,Y}\}, \quad (43)$$

and

$$\beta_0(h) \equiv \frac{\alpha_c \alpha_m}{s_i} = \frac{1}{16} \left[\frac{s_c s_m}{s_i} - (1 - 2h)^2 s_i + (1 - 2h)(s_c - s_m) \right], \quad (44)$$

$$\beta_m(h) \equiv \frac{\alpha_c s_m}{s_i} = \frac{1}{4} \left[\frac{s_c s_m}{s_i} - (1 - 2h)s_m \right], \quad (45)$$

$$\beta_c(h) \equiv \frac{\alpha_m s_c}{s_i} = \frac{1}{4} \left[\frac{s_c s_m}{s_i} - (1 - 2h)s_c \right]. \quad (46)$$

A full derivation is given in [13]. This curve is shown in Fig. 14.

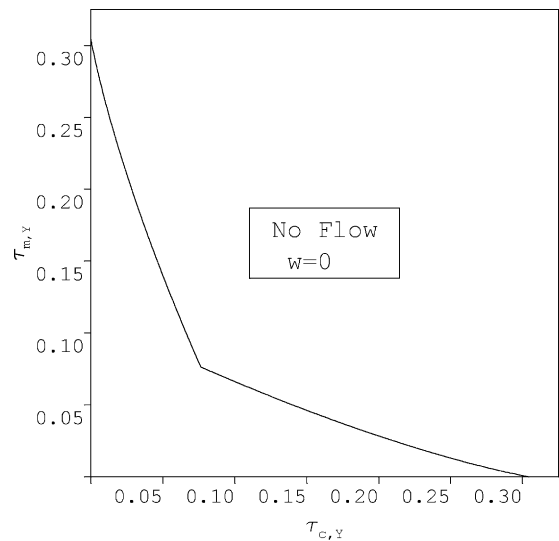


Fig. 14. The no-flow curve (42).

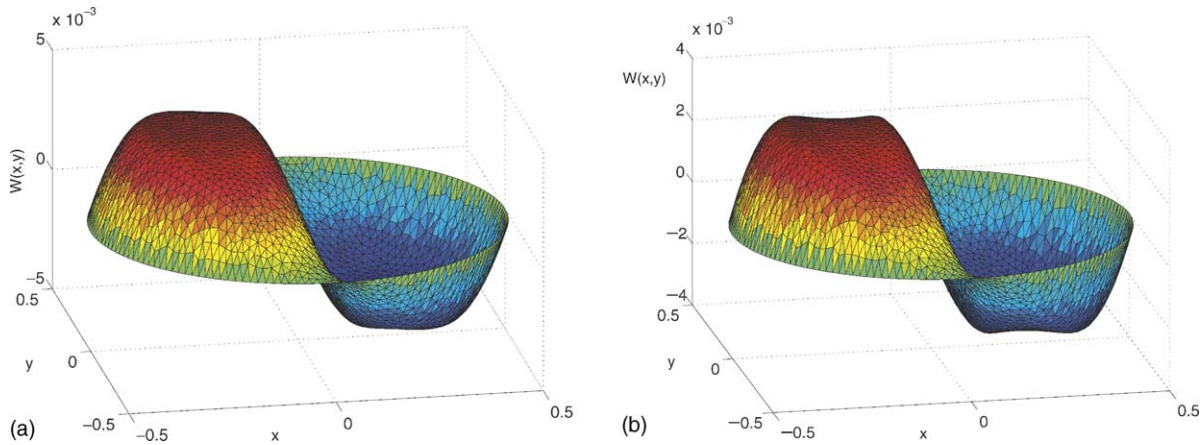


Fig. 15. Two examples of the exchange flow at $h = 0.5$, $\mu_c = \mu_m = 1$, $f = 0.5$: (a) $\tau_{c,Y} = \tau_{m,Y} = 0.035$, (b) $\tau_{c,Y} = \tau_{m,Y} = 0.04$.

3.3.1. Numerical test results

The objective of our numerical tests is to show that the augmented Lagrangian method can be effectively used to determine complex multi-fluid stopping criteria, such as (42).

We see from Fig. 14 that (42) is symmetrical about the line $\tau_{c,Y} = \tau_{m,Y}$. The intersection of (42) with the line $\tau_{c,Y} = \tau_{m,Y}$ can be determined analytically. If $\tau_{c,Y} = \tau_{m,Y}$, then by symmetry the maximum value of $F(h, \tau_{c,Y}, \tau_{m,Y})$ is at $h = 0.5$. Consequently, the intersection is:

$$\tau_{c,Y} = \tau_{m,Y} = \frac{1}{(16/\pi) + 8} = 0.07637\dots \tag{47}$$

In order to compute this limit with $\mu_c = \mu_m = 1$, we note that the flow should be symmetric, (i.e. up and down the duct), and that therefore the pressure gradient is $f = 0.5$. Note that in general, one would need to iterate the solution with respect to f , to ensure that (38) is satisfied. This is an unnecessary additional computational task which we have eliminated by selecting this symmetric case as a test.

Fig. 15 shows two examples of the velocity profile computed, quite far from the critical yield stresses. As the yield stresses increase towards the limiting values in (47), the yielded regions in Fig. 15 thin into boundary layers. We compute the stopping limit by examining the decay of Q_m with increasing yield stresses. Our numerical value is $\tau_{c,Y} = \tau_{m,Y} \approx 0.08$ which compares reasonably with the theoretical limit (47).

As a second example, we consider the zero flow limit when $\tau_{m,Y} = 0$ and $h = 0$. It is clear that the mud, which is now Newtonian, will flow unless $f = 0$. Thus, instead of approaching the zero flow limit by increasing the yield stresses while maintaining zero flux, we fix f and increase only $B = \tau_{c,Y}$, monitoring $Q(w)$, i.e. again we avoid the iteration with respect to f needed for the general problem. From (42) and (43), we can compute the theoretical limit of $B = \tau_{c,Y} = 0.25$. Fig. 16a shows an example velocity profile, close to the zero flow limit, and Fig. 16b shows the decay of $Q(w)$ as $B \rightarrow 0.25$. It is interesting to note that the cement flow is unyielded across most of the interface. There is no

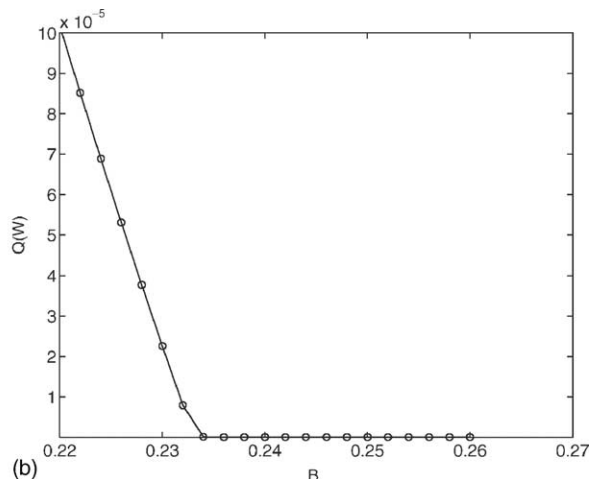
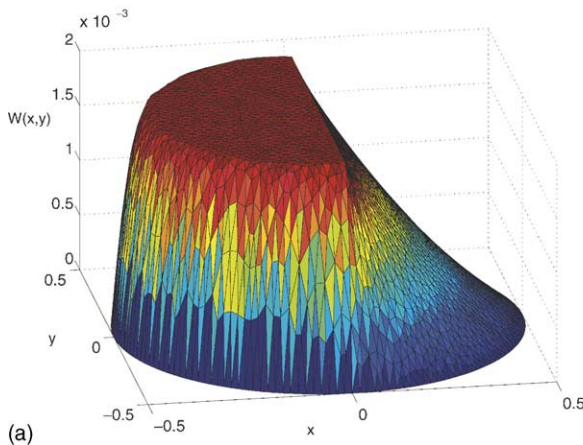


Fig. 16. Zero flow for $h = 0.5$, $\mu_c = \mu_m = 1$, $\tau_{m,Y} = 0$, $f = 0.0$: (a) velocity profile close to the zero flow limit, $B = \tau_{c,Y} = 0.2$; (b) decay in $Q(w)$ with $B = \tau_{c,Y}$, close to the theoretical limit of $\tau_{c,Y} = 0.25$.

pressure gradient driving the mud flow, so that the mud velocity profile is effectively a Couette profile.

4. Discussion and conclusions

In this paper we have demonstrated the utility of the augmented Lagrangian method for computing various zero flow limits, and related problems, for both single and multiple fluid duct flows. For such problems, regularisation methods are simply not suited, since they never produce zero flow. To our knowledge, our results are also some of the first multi-fluid visco-plastic computations to be carried out using this method.

The extension from single to multi-fluid flows is here straightforward for this restricted set of problems, both theoretically and computationally, and we have therefore restricted ourselves to a cursory description of the implementation. In computing more general multi-fluid problems, it is clear that we will encounter the full range of difficulties common to other fluid flows.

In particular, we have not considered surface tension effects explicitly. For the class of duct flows that we consider, inclusion of surface tension does not in fact change the mathematical problem: there is a pressure discontinuity between domains, related to interface shape, but since the shape of the domains is invariant in the z direction, the axial pressure gradients are identical. It is a different question whether or not such flows are realistic with the inclusion of surface tension. If we move to a multi-dimensional setting, but still remaining with steady flows, (e.g. slow steady bubble rise with surface tension), then the variational form is modified by the inclusion of an (interfacial) surface integral term. Since the interface remains fixed for the computation, the additional term is simply an additional linear functional and there is no particular problem mathematically. Indeed, problems of this type do arise in contact and friction problems, and can be handled numerically by similar methods, see e.g. [18]. At the next stage of complexity however, when the interface is allowed to move and perhaps also inertial terms are included, we have the full complexity of any multi-fluid problem.

Although for the problems we have examined, the regularised methods are inferior, it does not discount their usage. One principal advantage is that viscosity regularisations can be implemented straightforwardly in standard iterative solvers for nonlinear problems (and in commercial CFD codes). Another advantage is in allowing greater scope for the solution of the nonlinear algebraic system. However, in our opinion there are also a number of nice features of the augmented Lagrangian method implemented by the Uzawa algorithm, (especially for problems as we have considered), which are often overlooked (or simply not appreciated). These we have discussed in Section 2.1.

For both algorithms, the main CPU cost of each iteration is in solving a linear (or linearised) Poisson equation, for which the CPU cost is similar. Thus, comparing CPU

cost is essentially comparing the number of iterations required for convergence. One example of this comparison has been given in Fig. 3b, which illustrates that the methods have similar costs. However, in general we have resisted making any more general statement on comparative CPU, and do not feel it is helpful to do so. Certainly, we have found the augmented Lagrangian method competitive with viscosity regularisations in our computations, but we have not made great efforts at improving efficiency of either method. It is difficult to make a comparison objectively. As the regularisation parameter $\epsilon \rightarrow 0$ in the regularised method, the solution algorithm generally becomes ill-conditioned, but convergence to the analytic solution occurs in this limit, (i.e. there is a trade-off and one has to choose ϵ that is *good enough*). This balance, in using the regularisation method, is determined by the problem at hand and will usually be problem specific. Essentially, this means there is an outer iteration on ϵ , (by hand and/or mind), if one wants to do this in a rational way.

Acknowledgements

The contribution of M.M.-G. has been supported through a graduate scholarship from Consejo Nacional de Ciencia y Tecnología (CONACYT) of Mexico, held at University of British Columbia. The research of I.F. is supported by NSERC Canada and the British Columbia Advanced Systems Institute (BCASI), through the award of a BCASI university research fellowship. We thank E. Piras and Prof. O. Scherzer for their useful insights and discussions.

References

- [1] E.C. Bingham, Fluidity and Plasticity, McGraw-Hill, New York, 1922, pp. 215–218.
- [2] J.G. Oldroyd, Two-dimensional plastic flow of a Bingham solid, Proc. Camb. Phil. Soc. 43 (1947) 383–395.
- [3] W. Prager, On Slow Visco-Plastic Flow, Chapter in Studies in Mathematics and Mechanics. Volume presented to Richard von Mises, Academic Press, 1954.
- [4] P.P. Mossolov, V.P. Miasnikov, Variational Methods in the theory of the fluidity of a viscous plastic medium, J. Mech. Appl. Math. 29 (3) (1965) 468–492.
- [5] P.P. Mossolov, V.P. Miasnikov, On stagnant flow regions of a viscous-plastic medium in pipes, J. Mech. Appl. Math. 30 (4) (1966) 705–717.
- [6] G. Duvaut, J.L. Lions, Inequalities in Mechanics and Physics, vol. 219, Springer-Verlag, 1976 pp. 279–327.
- [7] R. Byron-Bird, G.C. Dai, B.J. Yarusso, The Rheology and Flow of Viscoplastic Materials, Rev. Chem. Eng. 1 (1) (1983) 2–70.
- [8] I.A. Frigaard, Stratified exchange flows of two Bingham fluids in an inclined slot, J. Non-Newtonian Fluid Mech. 78 (1998) 61–87.
- [9] I.A. Frigaard, O. Scherzer, Uniaxial exchange flows of two Bingham fluids in a cylindrical duct, IMA J. Appl. Math. 61 (1998) 237–266.
- [10] H. Fenie, I.A. Frigaard, Preventing buoyancy driven flows of two Bingham fluids in a closed pipe: fluid rheology design for oilfield plug cementing, Math. Comput. Modelling 30 (7–8) (1999) 71–91.
- [11] I.A. Frigaard, J. Crawshaw, Preventing buoyancy driven flows of two Bingham fluids in a closed pipe: fluid rheology design for oilfield plug cementing, J. Eng. Math. 36 (1999) 327–348.

- [12] M. Allouche, I.A. Frigaard, G. Sona, Static wall layers in the displacement of two visco-plastic fluids in a plane channel, *J. Fluid Mech.* 424 (2000) 243–277.
- [13] I.A. Frigaard, O. Scherzer, The effects of yield stress variation on uniaxial exchange flows of two Bingham fluids in a cylindrical duct, *SIAM J. Appl. Math.* 60 (6) (2000) 1950–1976.
- [14] I.A. Frigaard, Super-stable parallel flows of multiple visco-plastic fluids, *J. Non-Newtonian Fluid Mech.* 100 (2001) 49–76.
- [15] M. Moyers-Gonzalez, I.A. Frigaard, C. Nouar, Visco-plastic lubrication of viscous shear flows. *J. Fluid Mech.*, November 2003, in press.
- [16] M. Fortin, R. Glowinski, *Augmented Lagrangian Methods*, North-Holland, 1983.
- [17] R. Glowinski, J.L. Lions and R. Tremolieres, *Numerical Analysis of Variational Inequalities*, vols. 1 and 2, North-Holland, Amsterdam, 1981; translated from the French version: *Analyse numérique des inéquations variationnelles*, Dunod, Paris, 1976.
- [18] R. Glowinski, *Numerical Methods for Nonlinear Variational Problems*, Springer-Verlag, 1983.
- [19] R.R. Huilgol, M.P. Panizza, On determination of the plug flow region in Bingham fluids through the application of variational inequalities. *J. Non-Newtonian Fluid Mech.* 58 (1995) 207–217.
- [20] R.H.W. Hoppe, G. Mazurkevitch, U. Rettig, O. von Stryk, *Modelling, Simulation and Control of Electrorheological Fluid Devices*. SFB-438–9917, preprint series, T.-U. München, 1999.
- [21] M. Bercovier, M. Engleman, A finite-element method for incompressible non-Newtonian flows, *J. Comp. Phys.* 36 (1980) 313–326.
- [22] T.C. Papanastasiou, Flows of materials with yield, *J. Rheol.* 31 (5) (1987) 385–404.
- [23] S.S. Abdali, E. Mitsoulis, N.C. Markatos, Entry and exit flows of Bingham fluids, *J. Rheol.* 36 (2) (1997) 389–407.
- [24] C.R. Beverly, R.I. Tanner, Numerical analysis of three-dimensional Bingham plastic flow, *J. Non-Newtonian Fluid Mech.* 42 (1992) 85–115.
- [25] J. Blackery, E. Mitsoulis, Creeping motion of a sphere in tubes filled with a Bingham plastic material, *J. Non-Newtonian Fluid Mech.* 70 (1997) 59–77.
- [26] T.C. Papanastasiou, A.G. Boudouvis, Flows of viscoplastic materials: models and computations, *Comput. Struct.* 64 (1-4) (1997) 677–694.
- [27] P. Szabo, O. Hassager, Flow of Viscoplastic Fluids in Eccentric Annular Geometries, *J. Non-Newtonian Fluid Mech.* 45 (1992) 149–169.
- [28] A.J. Taylor, S.D.R. Wilson, Conduit flow of an incompressible yield stress fluid, *J. Rheol.* 41 (1) (1997) 93–101.
- [29] I.C. Walton, S.H. Bittleston, The Axial Flow of a Bingham Plastic in a Narrow Eccentric Annulus, *J. Fluid Mech.* 222 (1991) 39–60.
- [30] Y. Wang, Finite element analysis of the duct flow of Bingham plastic fluids: an application of the variational inequality, *Int. J. Num. Meth. Fluids.* 25 (1997) 1025–1042.
- [31] A.N. Beris, J.A. Tsamopoulos, R.C. Armstrong, R.A. Brown, Creeping motion of a sphere through a Bingham plastic, *J. Fluid Mech.* 158 (1985) 219–244.
- [32] N. Roquet, P. Saramito, An adaptive finite element method for viscoplastic fluid flows in pipes, *Comput. Meth. Appl. Mech. Eng.* 190 (2000) 5391–5412.
- [33] C.-S. Yih, Instability due to viscosity stratification, *J. Fluid Mech.* 27 (2) (1967) 337–352.
- [34] C.E. Hickox, Instability due to viscosity and density stratification in axisymmetric pipe flow, *Phys. Fluids* 14 (2) (1971) 251–262.
- [35] A.P. Hooper, W.G. Boyd, Shear flow instability due to a wall and a viscosity discontinuity at the interface, *J. Fluid Mech.* 179 (1987) 201–225.
- [36] S.G. Yiantsos, B.G. Higgins, Linear stability of plane Poiseuille flow of two superposed fluids, *Phys. Fluids* 31 (1988) 3225–3238.
- [37] D.D. Joseph, Y.Y. Renardy, *Fundamentals of two-fluid dynamics*, Interdisciplinary Applied Mathematics, Springer, 1993.
- [38] E.J. Hinch, A note on the mechanism of the instability at the interface between two shearing fluids, *J. Fluid Mech.* 114 (1984) 463–465.
- [39] F. Charru, “Phase diagram” of interfacial instabilities in two-layer shear flows, in: *Proceedings of the Third International Conference on Multiphase Flow, ICMF’98*, Lyon, France, 8–12 June 1998.
- [40] N.D. Waters, The stability of two stratified power law fluids in Couette flow, *J. Non-Newt. Fluid Mech.* 12 (1983) 85–94.
- [41] N.D. Waters, A.M. Keeley, The stability of two stratified non-Newtonian liquids in Couette flow, *J. Non-Newt. Fluid Mech.* 24 (1987) 161–181.
- [42] B. Khomami, Interfacial stability and deformation of two stratified power law fluids in plane Poiseuille flow, Part 1. stability analysis, *J. Non-Newt. Fluid Mech.* 36 (1990) 289–303.
- [43] Y.Y. Su, B. Khomami, Stability of multi-layer power law and second order fluids in plane Poiseuille flow, *Chem. Eng. Commun.* 109 (1991) 209–223.
- [44] A. Pinarbasi, A. Liakopoulos, Stability of two-layer Poiseuille flow of Carreau–Yasuda and Bingham-like fluids, *J. Non-Newtonian Fluid Mech.* 57 (1995) 227–241.
- [45] E. Comparini, P. Mannucci, Flow of a Bingham fluid in contact with a Newtonian fluid, *J. Math. Anal. Appl.* 227 (1998) 359–381.
- [46] D.G. Calvert, J.F. Heathman, J.E. Griffith, *Plug Cementing: Horizontal to Vertical Conditions*. Society of Petroleum Engineers, Paper number SPE 30514, 1995.